

# Imputation of Unknown Missingness in Sparse Electronic Health Records

Jun Han\* Josue Nassar\* Sanjit Singh Batra\*  
Aldo Cordova-Palomera Vijay Nori Robert E. Tillman

\* Equal Contribution  
Optum AI

{jun\_han, josue\_nassar, sanjit.batra, aldop, vijay.nori, rob.tillman}@optum.com

## Abstract

Machine learning holds great promise for advancing the field of medicine, with electronic health records (EHRs) serving as a primary data source. However, EHRs are often sparse and contain missing data due to various challenges and limitations in data collection and sharing between healthcare providers. Existing techniques for imputing missing values predominantly focus on *known unknowns*, such as missing or unavailable values of lab test results; most do not explicitly address situations where it is difficult to distinguish what is missing. For instance, a missing diagnosis code in an EHR could signify either that the patient has not been diagnosed with the condition or that a diagnosis was made, but not shared by a provider. Such situations fall into the paradigm of *unknown unknowns*. To address this challenge, we develop a general purpose algorithm for denoising data to recover unknown missing values in binary EHRs. We design a transformer-based denoising neural network where the output is thresholded adaptively to recover values in cases where we predict data are missing. Our results demonstrate improved accuracy in denoising medical codes within a real EHR dataset compared to existing imputation approaches and leads to increased performance on downstream tasks using the denoised data. In particular, when applying our method to a real world application, predicting hospital readmission from EHRs, our method achieves statistically significant improvement over all existing baselines.

## Introduction

Previous work has demonstrated the potential of applying machine learning to the medical domain for tasks such as disease prediction, clinical trial design, and health economics and outcome research (Deng et al. 2021; Liu et al. 2021; Padula et al. 2022). A standard data source for ML in the medical domain is electronic health records (EHRs). Additionally, many existing disease prediction models primarily utilize tabular formats, often transforming longitudinal EHR data into binary or categorical forms, rather than employing time-series forecasting methods (Lee et al. 2022; Huang et al. 2021; Rao et al. 2023; Debal and Sitote 2022).

In practice however, EHRs, upon being binarized, are prone to having missing values due to a variety of reasons such as recording issues (Goldstein et al. 2017) and under-reporting (Chen et al. 2023). Moreover, the lack of data shar-

ing between providers and the heterogeneity of EHR coding across institutions (Hur et al. 2022) amplifies this problem as EHR records for the same patient can vary across providers and institutions. Training on EHR data in the presence of missingness can negatively impact model performance at test time. Therefore, to ensure the efficacy of trained models, it is beneficial to pre-process the data by replacing missing values.

The *de facto* approach for replacing missing values in data is via imputation (Rubin 1978; Gelman et al. 2004; Mazumder, Hastie, and Tibshirani 2010), where missing values are replaced with imputed values computed using available data. Generally, imputation techniques are designed for the *known unknown* scenario where it is known which fields are missing (Figure 1A). For instance, a lab test was ordered by the physician, but the value was not recorded or made available in the EHR. In practice, missing fields are commonly encoded with a special symbol to indicate that the value is missing, e.g., NaN (Li et al. 2021) or  $-1$  for binary data that is otherwise 0 or 1.

In contrast, clinical codes in EHRs encoded as tabular data are typically represented as 1 in the presence of a diagnosis code and represented as 0 in the absence of a diagnosis code. This binary representation can be ambiguous as a 0 corresponding to a specific diagnosis code may indicate that the patient does not have the diagnosis **or** they do, but it is missing. For example, suppose that the ICD code corresponding to diabetes is represented as 0 in a tabular encoding of a patient’s EHR. Without additional supporting evidence, this could mean either: 1) that the patient **has not** been diagnosed with diabetes, i.e., a negative diagnosis or 2) that the patient **was** diagnosed with diabetes by a physician, but this diagnosis was not recorded by the physician or made available in the EHR. Thus, unlike the known unknowns paradigm, it is unclear when data are missing. We therefore refer to this scenario as *unknown unknowns* (Figure 1B). This ambiguity makes the problem of imputation significantly more challenging, as it necessitates determining whether an absent code should be treated as missing or not, significantly increasing the complexity of the solution space (Figure 1B). Moreover, recent works have shown that the missingness of negative diagnosis is a much more common issue in EHRs compared to the missingness of positive diagnosis codes (Wu et al. 2023; Chen et al. 2023). While one could treat all codes of value 0

as missing and apply traditional imputation approaches, the sparsity of EHRs prevents such a strategy from being a viable solution.

In this work, we propose an approach, Denoise2Impute, based on denoising, that allows for better recovery of unknown unknowns compared to SOTA imputation-based approaches. Denoise2Impute, is a denoising neural network parameterized by a SetTransformer (Lee et al. 2019) that allows the model to learn relationships between different ICD codes, e.g., a positive diabetes diagnosis is correlated with high glucose. While Denoise2Impute performs well, to increase its ability to distinguish whether a 0 corresponds to a negative diagnosis or a missing diagnosis code, we systematically formulate this challenge of unknown unknowns in EHRs as a denoising problem and theoretically derive the optimal denoising function. Inspired by the theory, we introduce an extension of Denoise2Impute, which we denote as Denoise2Impute-T, where data-dependent thresholds are computed to help stabilize the output of the network. To assess the efficacy of our proposed approach, we compute the accuracy of the resulting denoising as well as perform comprehensive evaluations on a variety of downstream tasks using the denoised data. We demonstrate that our proposed approach outperforms baselines by  $\sim 2\%$  AUPRC in denoising clinical codes within a large EHR dataset and the denoised EHRs outperform baseline approaches on a variety of clinical prediction tasks by  $\sim 0.5\%$ .

## Related Work

**Imputation and Denoising** The process of denoising data sources has been extensively investigated with numerous domain-specific methods proposed (Brown and Hwang 1997; Buades, Coll, and Morel 2005; Mazumder, Hastie, and Tibshirani 2010; Stekhoven and Bühlmann 2012; Jarrett et al. 2022; You et al. 2020; Peis, Ma, and Hernández-Lobato 2022), particularly in the medical domain (Chowdhury, Islam, and Khan 2017; Liu et al. 2023). When it is known which entries are corrupted or missing, the denoising problem reduces to imputation, for which various techniques have been developed. In particular, K-nearest neighbor methods (Beretta and Santaniello 2016; Bai, Mangathayaru et al. 2022; Faisal and Tutz 2021), deep generative modeling approaches like variational autoencoders (Beaulieu-Jones, Moore, and CONSORTIUM 2017; Ma et al. 2018), and generative adversarial networks (Yoon, Jordon, and Schaar 2018; Luo et al. 2018). Techniques for imputation of time series medical data have been developed using diffusion models (Alcaraz and Strodthoff 2022; Lee and Park 2022; Zheng and Charoenphakdee 2022), and for the imputation of medical records using graph-based methods (Vivar et al. 2020; Vinas, Zheng, and Hayes 2021). These methods have been further refined by incorporating attention-based approaches, which leverage learned correlations among known features to impute missing data (Lewis et al. 2021; Yıldız, Koç, and Koç 2022; Wang et al. 2022; Festag and Spreckelsen 2023). In (Chen et al. 2023), an imputation algorithm based on interpretable machine learning was devised to allow for performant and interpretable imputation algorithms.

**Unknown Unknowns** The problem of unknown unknowns has been studied in various domains, where it has also been referred to as latent missingness (Wu et al. 2023), under-reported variables (Sechidis et al. 2017) and data with positive and unlabeled data (Lazkecka, Mielniczuk, and Teisseyre 2021). In Wu et al. (2023), an active learning procedure for unknown unknowns in EHRs was proposed that takes into account the cost of checking if an absent diagnosis code is missing or negative. Sechidis et al. (2017) and Lazkecka, Mielniczuk, and Teisseyre (2021) both focus on the classification setting where the label and/or the features can have unknown unknowns. While similar in spirit to our proposed approach, these approaches are not scalable as they rely on computing conditional probabilities which is infeasible for EHRs as they can have  $\sim 1,000$  diagnosis codes. In (Suleiman et al. 2020), domain knowledge from expert clinicians is used to devise a recommender-system approach for imputing unknown unknowns in EHR data; we consider this work complimentary to ours. In Wu et al. (2016), a recommender-based system built on denoising autoencoders was to handle the cases of unknown unknowns in user preferences; we consider this work complimentary to ours. Another domain that deals with unknown unknowns is genomics, One class of approaches utilizes multiple noisy instances of a DNA sequence to build a denoised consensus sequence (Edgar and Flyvbjerg 2015; Wenger et al. 2019). Another class of denoising approaches for DNA sequences utilizes additional covariates to perform denoising (Wang et al. 2020). In this paper, however, we focus on denoising when there is a single noisy data point where it is not known *a priori* which fields of the data point are corrupted or missing.

## Denoise2Impute: Denoising Unknown Unknowns in EHRs

**Background and Notation** We begin by introducing notation and reviewing the goal of denoising. Let  $\mathbf{x}$  denote noiseless data, where  $\mathbf{x} \sim p(\mathbf{x})$ ,  $\mathbf{x} \in \mathcal{X}$ . Let  $\tilde{\mathbf{x}} \sim p(\tilde{\mathbf{x}} | \mathbf{x})$ ,  $\tilde{\mathbf{x}} \in \tilde{\mathcal{X}}$  denote the corresponding noisy data where  $p(\tilde{\mathbf{x}} | \mathbf{x})$  is the noise distribution that describes the corruption process, e.g.,  $p(\tilde{\mathbf{x}} | \mathbf{x}) = \mathcal{N}(\tilde{\mathbf{x}} | \mathbf{x}, \sigma^2 I)$ . The goal of denoising is to learn a function,  $g_\theta : \tilde{\mathcal{X}} \rightarrow \mathcal{X}$ , with parameters  $\theta$ , that can recover  $\mathbf{x}$  from  $\tilde{\mathbf{x}}$ , i.e.,  $\hat{\mathbf{x}}_\theta = g_\theta(\tilde{\mathbf{x}})$ . Given a dataset of noisy and noiseless pairs,  $\mathcal{D} = \{(\tilde{\mathbf{x}}_i, \mathbf{x}_i)\}_{i=1}^N$ , we train  $g_\theta$  by minimizing a loss function that is appropriate for the data modality.

EHRs are commonly represented as binary vectors,  $\tilde{\mathbf{x}} = [\tilde{x}_1, \dots, \tilde{x}_d, \dots, \tilde{x}_T]$ , and  $\mathbf{x} = [x_1, \dots, x_d, \dots, x_T]$ , where  $\tilde{x}_d, x_d \in \{0, 1\}$ . Given an ICD code from the noisy patient EHR,  $\tilde{x}_d$ , there are two possible scenarios when performing imputation of unknown unknowns. If  $\tilde{x}_d = 1$ , then we preserve it as we assume that there is no ambiguity for positive diagnosis. If  $\tilde{x}_d = 0$ , then denoising is done to infer whether the 0 is a negative diagnosis or a missing positive diagnosis.

When a clean EHR dataset is available, we propose to train a transformer-based denoising neural network,  $g_\theta$ , taking noisy EHR of a patient as input during training, which can be obtained by masking the clean data, and predicting the complete EHR. The transformer-based denoising neural

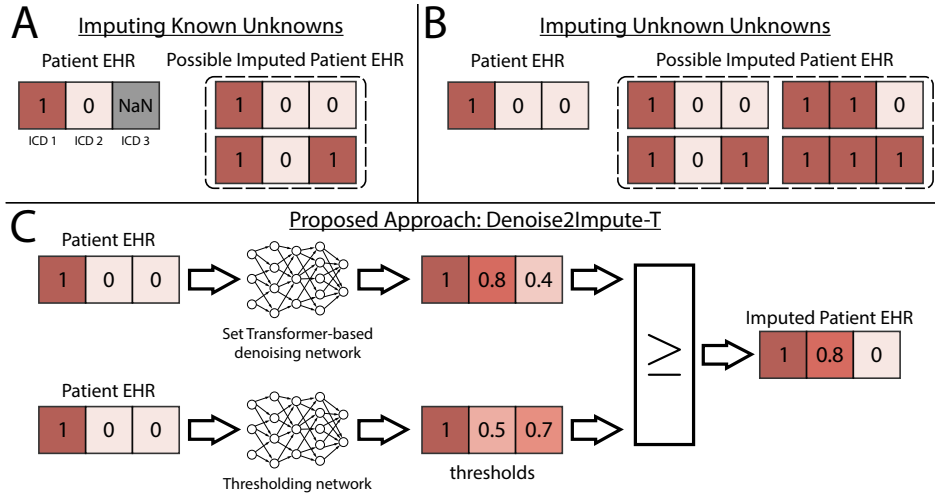


Figure 1: **A)** An example of imputing known unknowns. In the patient EHR, there is NaN in ICD 3. Thus, there are only two possible choices for ICD 3: 0 or 1. **B)** An example of imputing unknown unknowns. In the patient EHR, there is a 0 in ICD 2 and ICD 3. Due to reporting issues, it is unclear whether a 0 represents a negative diagnosis (0) or a missing diagnosis (1). Due to this ambiguity, there are 4 possibilities after imputing: i) ICD 2 and 3 are both negative diagnoses, thus they both are 0. ii) ICD 2 was missing, thus it is 1. ICD 3 was a negative diagnosis, thus it is a 0. iii) ICD 2 was a negative diagnosis, thus it is a 0. ICD 3 was missing, thus it is 1. iv) Both ICD 2 and 3 are missing, thus they both are 1. **C)** Our proposed approach, Denoise2Impute-T, comprises 2 components. A patient EHR is input into a Set Transformer based denoiser that outputs a denoised patient EHR. The EHR is also input into a Thresholding network that outputs thresholds for each ICD code. A *greater than or equal to* element-wise comparison is performed between the denoised EHR and the thresholds, that leads to the final imputed EHR.

network learns the correlation between different dimensions of EHRs in order to predict the true missing values in EHRs; we call our proposed approach Denoise2Impute.

We begin by discussing the motivation for the choice of the Set Transformer for parametrizing  $g_{\theta}$ . As mentioned previously, a 0 for an ICD code in the noisy EHR could mean that the same ICD code in the noiseless EHR could either be a 0 or a 1. Thus, to perform well, it is crucial for the network to learn and leverage relationships between diagnosis codes. As an example, suppose that in a patient’s EHR we see there is a 0 for the diabetes ICD code. Patients with obesity and high glucose are also likely to have diabetes. Thus, if a 1 is present for both the obesity and high glucose ICD codes, but a 0 is present for the diabetes code, then it is likely that there is a missing diabetes diagnosis. In contrast, if the patient has a clean bill of health and there is a 0 present for the diabetes code, it is likely that there is not a missing diabetes diagnosis.

For learning this relationship, we parameterize  $g_{\theta}$  with a Set Transformer (Lee et al. 2019), as they have been shown to be able to learn pairwise and higher-order interactions between the dimensions of an input. Moreover, unlike standard transformers, the Set Transformer architecture is agnostic to the order of the input, alleviating the need to design a positional encoding scheme for ICD codes (which is non-trivial).

For binary data, a natural choice for the loss function is the element-wise cross entropy (CE) loss

$$\ell_{CE}(g_{\theta}(\tilde{\mathbf{x}}_i), \mathbf{x}_i) = \sum_{d=1}^T \ell_{ce}(g_{\theta}(\tilde{\mathbf{x}}_i)_d, x_{i,d}), \quad (1)$$

where  $g_{\theta}(\tilde{\mathbf{x}}_i)_d$  is the  $d$ -th dimension of  $g_{\theta}(\tilde{\mathbf{x}}_i)$  and

$$\ell_{ce}(g_{\theta}(\tilde{\mathbf{x}}_i)_d, x_{i,d}) = x_{i,d} \log g_{\theta}(\tilde{\mathbf{x}}_i)_d + (1 - x_{i,d}) \log(1 - g_{\theta}(\tilde{\mathbf{x}}_i)_d).$$

We found that when using (1) for training, the network underperformed on examples where  $\tilde{x}_{i,d} = 0$  and  $x_{i,d} = 1$ . Thus, we modified the loss function to put more weight on these instances

$$\tilde{\ell}_{CE}(g_{\theta}(\tilde{\mathbf{x}}_i), \mathbf{x}_i; \lambda) = \sum_{d=1}^T \mathbb{I}[\tilde{x}_{i,d} = x_{i,d}] \ell_{ce}(g_{\theta}(\tilde{\mathbf{x}}_i)_d, x_{i,d}) + \lambda \mathbb{I}[\tilde{x}_{i,d} \neq x_{i,d}] \ell_{ce}(g_{\theta}(\tilde{\mathbf{x}}_i)_d, x_{i,d}),$$

where  $\lambda$  is a hyperparameter that dictates how much emphasis we should place on training examples where  $\tilde{x}_{i,d} = 0$  and  $x_{i,d} = 1$ .

### Denoise2Impute-T: A theoretically motivated extension

While Denoise2Impute was generally effective at imputing unknown unknowns, we found instances where it struggled to discern whether a 0 was missing or a negative diagnosis. We hypothesized that this is in part due to the difficulty of the problem. Classically, when performing denoising we often assume—implicitly or explicitly—that we can discriminate between noiseless data,  $\mathbf{x}$ , and noisy data,  $\tilde{\mathbf{x}}$ . Intuitively, this makes sense; we only perform denoising if the data is noisy, i.e.,  $\tilde{\mathbf{x}} \neq \mathbf{x}$ . If a data point is not noisy, i.e.,  $\tilde{\mathbf{x}} = \mathbf{x}$ , then no denoising is performed, i.e.,  $g_{\theta}$  is the identity function.

In the *unknown unknowns* scenario, it is no longer easy to discriminate between  $\tilde{\mathbf{x}}$  and  $\mathbf{x}$ . For example, in the case of EHRs it is difficult to discriminate between  $\tilde{\mathbf{x}}$  and  $\mathbf{x}$  as 1) EHRs are generally very sparse and 2) the absence of a code can either mean that the patient was not diagnosed with that disease or that the patient was diagnosed but the code was not recorded or is unavailable in the EHR. Thus, given a sparse EHR vector it is difficult to discern whether it is noiseless or whether it should be denoised. Intuitively, we would expect denoising in the unknown unknowns scenario to be difficult as now we must discern which points need to be denoised. While in principle, we could denoise every 0, this may introduce artifacts into the data, especially when the data are sparse (Tanner, Morgan-Short, and Luck 2015) and lead to suboptimal performance.

To formalize the intuition presented above, we begin by restricting ourselves to the case where  $\mathcal{X} \subseteq \mathbb{R}^T$  and  $\tilde{\mathcal{X}} \subseteq \mathbb{R}^T$  and write the noise distribution,  $p(\tilde{\mathbf{x}} | \mathbf{x})$ , as follows:

$$p(\tilde{\mathbf{x}} | \mathbf{x}) = \beta \delta(\tilde{\mathbf{x}} = \mathbf{x}) + (1 - \beta)q(\tilde{\mathbf{x}} | \mathbf{x}), \quad (2)$$

where  $\delta(\cdot)$  is the Dirac delta function and  $\beta \in [0, 1]$ . With (2) we attempt to model the unknown unknowns setting, where with probability  $\beta$  no noise is added, i.e.,  $\tilde{\mathbf{x}} = \mathbf{x}$ , and with probability  $1 - \beta$  noise is introduced via  $q(\tilde{\mathbf{x}} | \mathbf{x})$ . (2) demonstrates the difficulty of the problem: if  $\beta$  is large then with high probability,  $\tilde{\mathbf{x}} = \mathbf{x}$ , making it impossible to discriminate between the two. Moreover, the form of  $q(\tilde{\mathbf{x}} | \mathbf{x})$  can also make the problem difficult as noise can be injected that can make  $\tilde{\mathbf{x}}$  likely under the data distribution,  $p(\mathbf{x})$ .

Given (2), we seek to derive the optimal denoising function,  $f_* : \tilde{\mathcal{X}} \rightarrow \mathcal{X}$ . Specifically, we seek the optimal denoising function that minimizes the expected mean squared error (MSE)

$$f_*(\cdot) = \underset{f(\cdot)}{\operatorname{argmin}} \mathbb{E}_{p(\mathbf{x})p(\tilde{\mathbf{x}}|\mathbf{x})} [(f(\tilde{\mathbf{x}}) - \mathbf{x})^\top (f(\tilde{\mathbf{x}}) - \mathbf{x})].$$

Using calculus of variations, we can derive the functional form of  $f_*$ . Due to space, we state an informal theorem below, which we prove in the Appendix.

**Theorem 1.** *Let  $p(\mathbf{x})$  be the data distribution, let  $p(\tilde{\mathbf{x}} | \mathbf{x})$  the noise distribution as defined in (2) and let  $q(\tilde{\mathbf{x}}) = \int q(\tilde{\mathbf{x}} | \mathbf{x})p(\mathbf{x})d\mathbf{x}$  the marginal distribution of the noisy data. With respect to MSE, the optimal denoising function is*

$$f_*(\tilde{\mathbf{x}}) = \omega(\tilde{\mathbf{x}})\tilde{\mathbf{x}} + (1 - \omega(\tilde{\mathbf{x}})) g_*(\tilde{\mathbf{x}}), \quad (3)$$

where

$$g_*(\tilde{\mathbf{x}}) \triangleq \mathbb{E}_{q(\mathbf{x}|\tilde{\mathbf{x}})}[\mathbf{x}], \omega(\tilde{\mathbf{x}}) \triangleq \frac{p(\tilde{\mathbf{x}})}{p(\tilde{\mathbf{x}}) + \gamma \tilde{q}(\tilde{\mathbf{x}})}, \gamma \triangleq \frac{1 - \beta}{\beta}.$$

From (3), we see that the optimal denoising function  $f_*$  is a convex combination of the identity function and the minimum MSE,  $g_*$  (Casella and Berger 2021), where the weight is determined by  $\omega(\tilde{\mathbf{x}}) \in [0, 1]$ . Specifically,  $\omega(\tilde{\mathbf{x}})$  measures how likely  $\tilde{\mathbf{x}}$  is under the data distribution  $p(\mathbf{x})$ , compared to the scaled marginal distribution of the noisy data  $\gamma \tilde{q}(\tilde{\mathbf{x}})$ . Denoising known unknowns corresponds to the case where it is easy to discriminate between  $p(\mathbf{x})$  and  $\gamma \tilde{q}(\tilde{\mathbf{x}})$ , corresponding to  $\omega(\tilde{\mathbf{x}}) \approx 0$  and  $\omega(\tilde{\mathbf{x}}) \approx 1$ . Denoising unknown unknowns

corresponds to the scenario where it is hard to discriminate between  $p(\mathbf{x})$  and  $\gamma \tilde{q}(\tilde{\mathbf{x}})$ , corresponding to  $p(\mathbf{x}) \approx \tilde{q}(\mathbf{x})$ ; this leads to  $\omega(\tilde{\mathbf{x}}) \approx \frac{1}{1+\gamma}$ . Thus,  $\gamma$  can be interpreted as a regularizer that allows us to choose how much weight  $f_*$  puts on the identity function or on the MMSE estimator which can lead to better behaved estimators.

Inspired by Theorem 1, we aim to extend Denoise2Impute. We cannot straightforwardly use Theorem 1 as (i) it requires knowledge of  $p(\mathbf{x})$ ,  $\beta$ , and  $q(\tilde{\mathbf{x}} | \mathbf{x})$ , which is usually not known and (ii) is designed for the MSE loss function, which assumes real-valued data, while we consider binary EHR data in this study. However, we conjecture that for many popular loss functions,  $\ell$ , the optimal denoising function can be written as

$$f_*(\tilde{\mathbf{x}}) = \omega(\tilde{\mathbf{x}})\tilde{\mathbf{x}} + (1 - \omega(\tilde{\mathbf{x}})) g_\ell(\tilde{\mathbf{x}}), \quad (4)$$

where the functional form of  $g_\ell : \tilde{\mathcal{X}} \rightarrow \mathcal{X}$ , depends on the choice of  $\ell$ , i.e. if  $\ell$  is MSE then  $g_\ell$  becomes the MMSE.

Inspired by (4), we can extend Denoise2Impute,  $g_\theta$ , by introducing a function that determines which codes to denoise. Specifically, given a trained denoiser,  $g_\theta$ , and a function,  $\omega_\phi$ , we can combine them to create a new denoising function,  $f$ , which we can be expressed as

$$f(\tilde{\mathbf{x}}) = \omega_\phi(\tilde{\mathbf{x}})\tilde{\mathbf{x}} + (1 - \omega_\phi(\tilde{\mathbf{x}})) g_\theta(\tilde{\mathbf{x}}). \quad (5)$$

We call (5) Denoise2Impute-T.

While there are many ways to parameterize  $\omega_\phi$ , we found the following to work well

$$\omega_\phi(\tilde{\mathbf{x}}) = \mathbb{I}[g_\psi(\tilde{\mathbf{x}}) < \phi], \quad (6)$$

where  $\mathbb{I}[\cdot]$  is the indicator function and  $\phi = [\phi_1, \dots, \phi_T]$  are learnable thresholds. The use of  $\phi$  allows Denoise2Impute-T to adaptively choose when to use the identity function or  $g_\psi$  for each individual dimension of  $\tilde{\mathbf{x}}$ . While the output of  $\omega$  in (3) is a scalar, we found that making it vector-valued, i.e. having a separate threshold for each dimension of  $\tilde{\mathbf{x}}$ , led to better empirical performance.

To train  $\omega_\phi$  we use a continuous relaxation of the indicator function and use  $()$  to compute the loss with respect to  $f$  (5)

$$\begin{aligned} \tilde{\ell}_{CE}(f(\tilde{\mathbf{x}}_i), \mathbf{x}_i; \lambda) &= \sum_{d=1}^T \mathbb{I}[x_{i,d} = \tilde{x}_{i,d}] \ell_{ce}(f(\tilde{\mathbf{x}}_i)_d, x_{i,d}) \\ &\quad + \lambda \mathbb{I}[x_{i,d} \neq \tilde{x}_{i,d}] \ell_{ce}(f(\tilde{\mathbf{x}}_i)_d, x_{i,d}), \end{aligned}$$

where  $g_\theta$  is kept fixed and only the parameters of  $\omega_\phi$  are updated. More details in training can be found in Appendix .

## Results

We include comprehensive experiments to demonstrate the accuracy and utility of our proposed methodology. First, we evaluate the denoising accuracy on a large EHR dataset. Next, the denoised EHRs are used in downstream prediction tasks. Below we provide brief details on the datasets and baselines. More details regarding data sources, model architectures and hyperparameters can be found in Appendix .

**Datasets** Payer companies and care delivery organizations (CDOs) commonly have overlapping patient population but have unique coding practices, i.e., the same patient’s EHR can differ between the payer company and the CDO. Thus, for training the denoising model, we begin with two sources of EHR data with overlapping patient populations from a large healthcare institute,  $\mathcal{D}_1 = \{\tilde{\mathbf{x}}_1, \dots, \tilde{\mathbf{x}}_N\}$  and  $\mathcal{D}_2 = \{\tilde{\mathbf{y}}_1, \dots, \tilde{\mathbf{y}}_M\}$ . Each data point is a vector of binary indicators for the presence of ICD-10 diagnosis codes in a patient’s EHR, where we set the number of codes to be 993, i.e.,  $T = 993$ . We leverage the overlapping patient populations of  $\mathcal{D}_1$  and  $\mathcal{D}_2$  to construct a dataset  $\mathcal{D}$  of size 445,345 patients. More details can be found in Appendix .

In Figure 2, we provide descriptive statistics for  $\mathcal{D}_1$  and  $\mathcal{D}_2$ . Figure 2A demonstrates that a majority of the 993 diagnosis codes have a prevalence of less than  $\sim 3\%$  for both  $\mathcal{D}_1$  and  $\mathcal{D}_2$ . Additionally, codes tend to have higher prevalence in  $\mathcal{D}_2$  than in  $\mathcal{D}_1$ . Figure 2B demonstrates the sparsity of patient EHRs, where for both  $\mathcal{D}_1$  and  $\mathcal{D}_2$ , a majority of patient EHRs have less than 6% of the ICD codes present. Furthermore, since each dot corresponds to a patient whose EHR is analyzed in  $\mathcal{D}_1$  and  $\mathcal{D}_2$ , we can compare the sparsity across the two datasets for each patient. We can therefore conclude that  $\mathcal{D}_1$  has a higher degree of sparsity in patient EHRs than  $\mathcal{D}_2$ .

While both  $\mathcal{D}_1$  and  $\mathcal{D}_2$  are very sparse, Figure 2C and 2D demonstrate a peak in eigenvalues of the covariance matrix of  $\mathcal{D}_1$  and  $\mathcal{D}_2$  compared to eigenvalues of the covariance matrix of random binary matrices (with prevalence matched to  $\mathcal{D}_1$  and  $\mathcal{D}_2$ , respectively). This suggests that  $\mathcal{D}_1$  and  $\mathcal{D}_2$  comprise higher-order structure across their dimensions which can then be leveraged by imputation methods to learn relationships between ICD-10 codes. Therefore,  $\mathcal{D}_1$  and  $\mathcal{D}_2$  provides versatile benchmarks to evaluate different methods.

In the final, we employ a real world dataset to evaluate our method on a popular healthcare prediction task from the literature, predicting hospital readmission from ICD-10 codes (Kansagara et al. 2011; Huang, Altosaar, and Ranganath 2019; Mahmoudi et al. 2020; Jiang et al. 2023). The size of the dataset is 1,670,347 of which the size of training dataset is 1,124,550 and the size of the testing dataset is 545,797. For the hospital readmission task, the trained denoising model is used to denoise a population of 1,670,347 patients which comes from the same source as  $\mathcal{D}_1$ .

**Baselines** We compare our two proposed approaches, Denoise2Impute and Denoise2Impute-T, against popular imputation methods wherein, for the imputation approaches all 0’s are treated as missing values. Specifically, we compare against the following imputation approaches: 1) replacing all 0’s with the **prevalence** computed by calculating mean for each dimension in  $\mathcal{D}_1$ , 2) k-nearest neighbor (**k-NN**) (with  $k = 5$ ) and 3) **softImpute** (Mazumder, Hastie, and Tibshirani 2010) using the implementation from Rubinsteyn and Feldman. We also compare the performance of Denoise2Impute but parametrized  $g_\theta$  with a feedforward neural network as opposed to a Set Transformer; this is denoted as **MLP**. We also compare against a denoising auto-encoder (**DAE**) and the collaborative denoising auto-encoders (**CDAE**) from Wu et al. (2016). We note that we attempted to compare against

the recommender-system based approach of (Suleiman et al. 2020), but their code was not publicly available. Training and architecture details can be found in Appendix .

**Benchmarking Imputation Performance** To investigate the imputation performance of all the methods, we compute the AUPRC between the imputed values and  $\mathcal{D}$  for each dimension. Table 1 summarizes the AUPRC averaged across all 993 dimensions. We observe that both Denoise2Impute and Denoise2Impute-T outperform the other methods, with Denoise2Impute-T achieving the the highest AUPRC and also improves upon using the original noisy data,  $\mathcal{D}_1$ .

In Figure 3, we investigate the performance of Denoise2Impute for denoising individual ICD codes. Specifically, we compare the dimension-wise AUPRC of the Denoise2Impute method against the prevalence (Figure 3A), not applying imputation and using  $\mathcal{D}_1$  as is (Figure 3B), and an MLP-parameterized Denoise2Impute (Figure 3C). In Figure 3A, we observe that the AUPRC of the denoised data using the Denoise2Impute is higher than the column mean (also referred to as *prevalence*) for each of the 993 dimensions. In Figure 3B, we observe that Denoise2Impute achieves higher AUPRC across all 993 dimensions than using the noisy data  $\mathcal{D}_1$  itself as the denoised data. In Figure 3C, we observe that using a Set Transformer to parametrize  $g_\theta$  in Denoise2Impute achieves higher AUPRC than using a feedforward neural network (referred to as MLP) in 866 ( $\sim 87\%$ ) out of the 993 dimensions.

Furthermore, to investigate how the noise distribution affects the performance of models, we created a synthetic noisy dataset from  $\mathcal{D}$ , where the noise was distributed such that the prevalence of the synthetic noisy dataset matches that of  $\mathcal{D}_1$ . The result on synthetic data in Figure 6 in Appendix shows consistent results with that of Figure 3. Together, both real and synthetic data experiments provide empirical support for the use of a Set Transformer within Denoise2Impute.

**Benchmarking Imputation on Downstream Tasks** We investigate how imputation performance can affect downstream task prediction, by benchmarking on two downstream tasks. Specifically, we first use the trained Denoise2Impute models to denoise the noisy data  $\mathcal{D}_1$  and then feed the denoised values into a downstream classifier (Ke et al. 2017).

To investigate whether the proposed approach was able to learn the relationship between diagnosis codes, we aim to predict a particular ICD code among the  $T$  codes given the others. To avoid information leakage, the target ICD code is set to 0 in the patient EHR before it is passed to the imputation methods. We begin by selecting six ICD codes for common chronic diseases and compute the difference in AUPRC with respect to using the original data,  $\mathcal{D}_1$ , along with 95% confidence intervals (Figure 4A). We observe that both Denoise2Impute and Denoise2Impute-T outperform all other methods for all six diseases, where Denoise2Impute-T tends to outperform Denoise2Impute. Interestingly, we found that softImpute often led to worse performance compared to using the original data,  $\mathcal{D}_1$ . The performance of softImpute suggests that treating all 0s as missing and performing imputation may lead to suboptimal performance in downstream tasks. In Figure 4B, we repeated the above experiment for

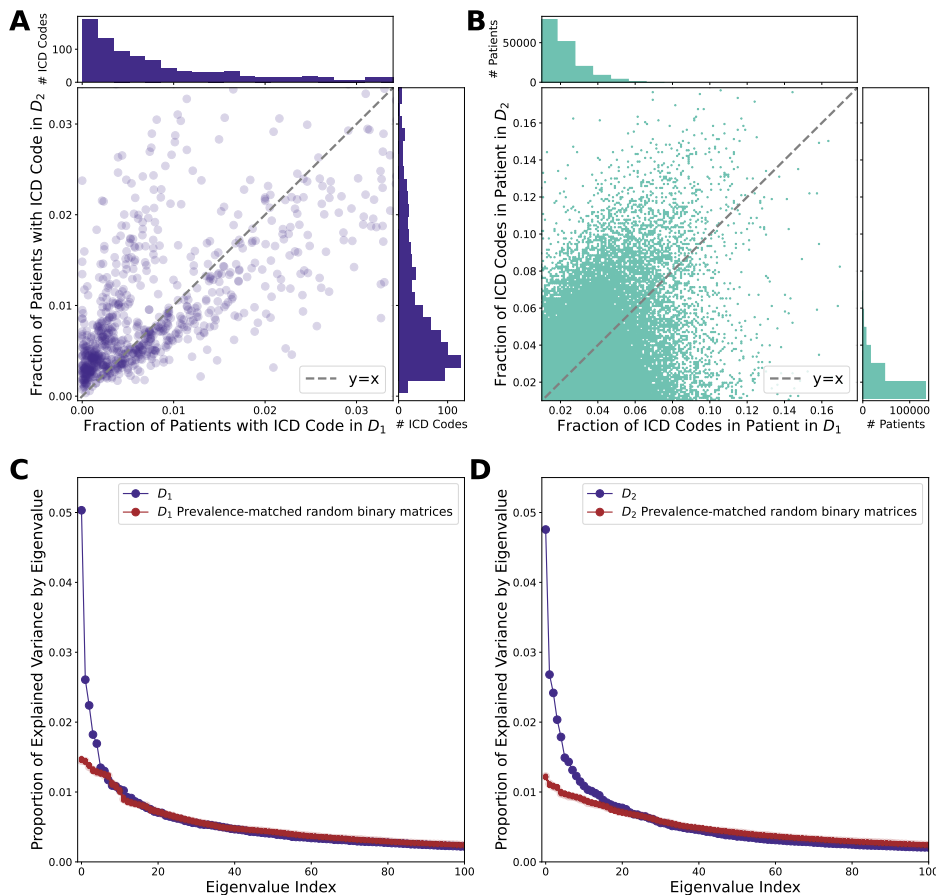


Figure 2: Descriptive statistics for both datasets used in this paper. **A)** Comparison of the prevalence of ICD codes in  $\mathcal{D}_1$  vs  $\mathcal{D}_2$ . **B)** Comparison of the sparsity of patient EHRs in  $\mathcal{D}_1$  vs  $\mathcal{D}_2$ . **C)** The eigenvalue spectra of the covariance matrix of  $\mathcal{D}_1$  (blue) with respect to 100 prevalence-matched random binary matrices (red). **D)** The eigenvalue spectra of the covariance matrix of  $\mathcal{D}_2$  (blue) with respect to 100 prevalence-matched random binary matrices (red).

Methods	$\mathcal{D}_1$	Prevalence	MLP	DAE	CDAE	D2Impute	D2Impute-T
Avg. AUPRC	51.86	52.37	61.91	62.05	62.17	64.90	<b>65.53</b>

Table 1: Average of dimension-wise AUPRC (higher is better) on the test set where noisy vectors were obtained from  $\mathcal{D}_1$ . D2Impute is short for Denoise2Impute.

eight additional randomly chosen ICD codes where we see the same trend as before; the description for the ICD codes can be found in Table 3 in Appendix .

Finally, we evaluate the performance on predicting hospital readmission, which is a popular clinical prediction task in the literature (Jiang et al. 2023; Kansagara et al. 2011; Huang, Altosaar, and Ranganath 2019; Mahmoudi et al. 2020). While ICD-10 codes can be used to predict hospital readmission, the fact that readmission prediction is not an ICD-10 code itself enhances its credibility as a benchmarking dataset since we no longer need to set a dimension to all 0s before performing denoising. In Figure 4C, we observe that both Denoise2Impute and Denoise2Impute-T achieve the highest AUPRC compared to the other methods in prediction of hospital readmission and that this increase is statistically signifi-

cant based on the 95% confidence intervals. Moreover, we see that the Denoise2Impute-T leads to a slight performance gain compared to Denoise2Impute but that this improvement is not statistically significant. Taken together, Denoise2Impute and Denoise2Impute-T outperform all existing imputation approaches on both, imputation and prediction tasks.

## Discussion

Missing data presents a substantial challenge for machine learning in the medical domain, as it can negatively impact performance and perpetuate existing disparities in health-care (Vyas, Eisenstein, and Jones 2020; Pierson et al. 2021). The problem becomes even more complex when the presence of missing entries is unclear. In response to this challenge, we introduced Denoise2Impute, a denoising-based approach

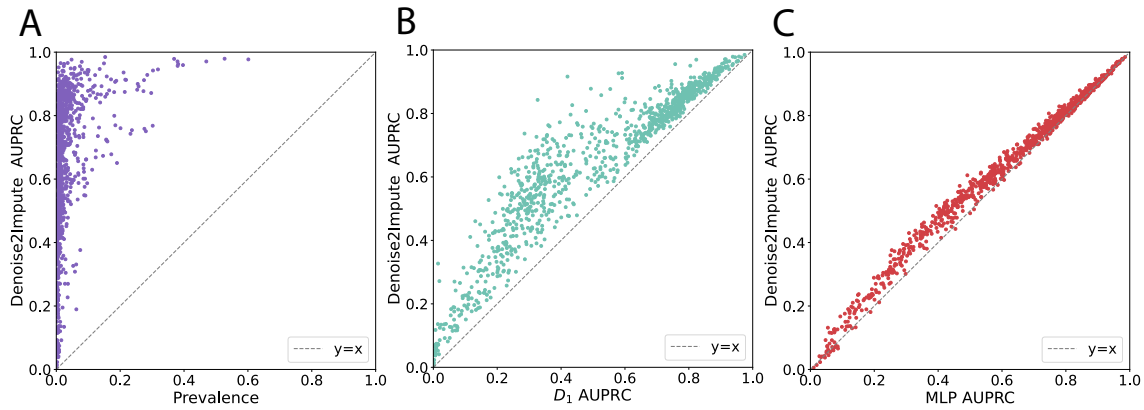


Figure 3: Dimension-wise AUPRC for  $T = 993$  computed on the test data. **A)** Comparison between AUPRC of the Denoise2Impute and the column mean (*prevalence*) for each dimension of the noisy data  $\mathcal{D}_1$ . **B)** Comparison between AUPRC of the Denoise2Impute and that of the  $\mathcal{D}_1$ . **C)** Comparison between AUPRC of the Denoise2Impute and AUPRC of the MLP.

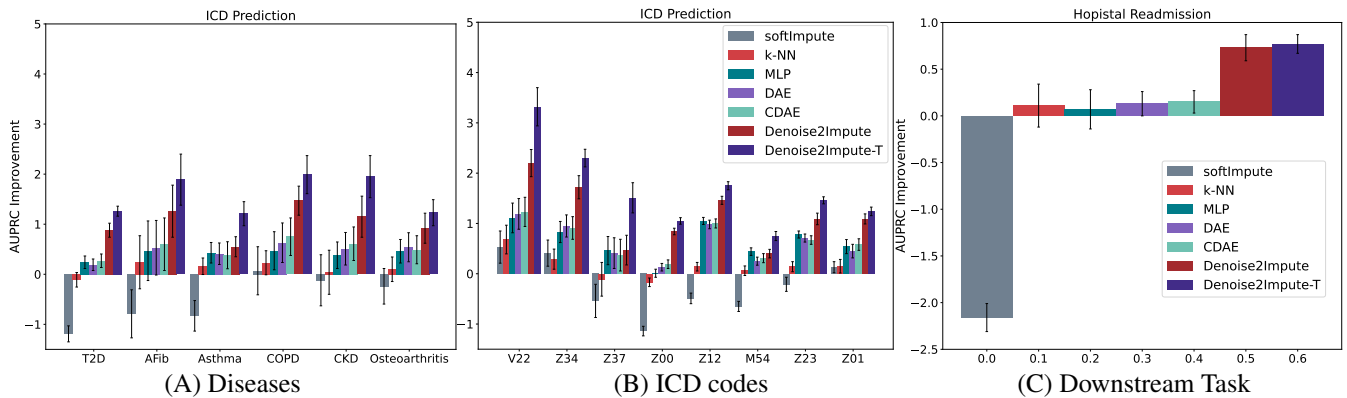


Figure 4: Results for ICD code prediction for six common chronic conditions (A) and eight randomly chosen ICD codes (B). Results for Hospital Readmission task (C). Difference in AUPRC relative to using  $\mathcal{D}_1$  and 95% confidence intervals are plotted. The common chronic conditions in (A) and the description of ICD codes in (B) are provided in Table 3 in Appendix .

that utilizes relationships between diagnosis codes to identify and impute missing codes effectively.

While our empirical evidence highlights Denoise2Impute’s effectiveness, we observed that certain diagnosis codes posed challenges for the approach. These difficulties may arise due to the extreme sparsity of some codes or insufficient training examples, making it hard for the model to learn useful dependencies between diagnosis codes. In such cases, Denoise2Impute’s output could introduce noise into the data, as the network struggles to differentiate between missing and existing diagnosis codes. To enhance the model’s performance, we developed a theoretically motivated extension called Denoise2Impute-T, which employs learned thresholds to regularize the model’s output. Our empirical results show that using learned thresholds with Denoise2Impute-T leads to performance gains over the original Denoise2Impute.

Despite these encouraging findings, there are limitations to our approach and opportunities for improvement. First, training Denoise2Impute necessitates a noiseless and noisy training set; while this may seem challenging, there are a

number of ways to obtain such a dataset. First, insurance companies and care delivery organizations (CDOs) commonly have overlapping patient population where an EHR for the same patient can differ between the insurance company and the CDO. Having access to these two dataset can allow for the creation of a noiseless dataset which can be used to train the model. Another approach is to create an artificial noisy dataset given a dataset of EHR’s via 0-1 binary masking, which is commonly employed in large language models (Devlin et al. 2018). Lastly, the approach of (Wu et al. 2023) can be used to allow for a cost-effective construction of a dataset of noisy and clean EHRs. Additionally, incorporating other tabular information, such as medications and laboratory results, could further enhance performance. Expanding the model to include multiple data modalities, like clinical text and the time-series component of EHR data, could provide a more comprehensive representation of patient history and lead to improved performance. For example, the threshold function  $\omega_\phi$  could be refined by considering additional information sources, allowing for patient-specific thresholding.

## References

- Alcaraz, J. L.; and Strothoff, N. 2022. Diffusion-based Time Series Imputation and Forecasting with Structured State Space Models. *Transactions on Machine Learning Research*.
- Bai, B. M.; Mangathayaru, N.; et al. 2022. Modified K-Nearest Neighbour Using Proposed Similarity Fuzzy Measure for Missing Data Imputation on Medical Datasets (MKN-NMBI). *International Journal of Fuzzy System Applications (IJFSA)*, 11(3): 1–15.
- Beaulieu-Jones, B. K.; Moore, J. H.; and CONSORTIUM, P. R. O.-A. A. C. T. 2017. Missing data imputation in the electronic health record using deeply learned autoencoders. In *Pacific symposium on biocomputing 2017*, 207–218. World Scientific.
- Beretta, L.; and Santaniello, A. 2016. Nearest neighbor imputation algorithms: a critical evaluation. *BMC medical informatics and decision making*, 16(3): 197–208.
- Brown, R. G.; and Hwang, P. Y. 1997. Introduction to random signals and applied Kalman filtering: with MATLAB exercises and solutions. *Introduction to random signals and applied Kalman filtering: with MATLAB exercises and solutions*.
- Buades, A.; Coll, B.; and Morel, J.-M. 2005. A non-local algorithm for image denoising. In *2005 IEEE computer society conference on computer vision and pattern recognition (CVPR'05)*, volume 2, 60–65. Ieee.
- Casella, G.; and Berger, R. L. 2021. *Statistical inference*. Cengage Learning.
- Chen, Z.; Tan, S.; Chajewska, U.; Rudin, C.; and Caruna, R. 2023. Missing Values and Imputation in Healthcare Data: Can Interpretable Machine Learning Help? In *Conference on Health, Inference, and Learning*, 86–99. PMLR.
- Chowdhury, M. H.; Islam, M. K.; and Khan, S. I. 2017. Imputation of missing healthcare data. In *2017 20th International Conference of Computer and Information Technology (IC-CIT)*, 1–6. IEEE.
- Debal, D. A.; and Sitote, T. M. 2022. Chronic kidney disease prediction using machine learning techniques. *Journal of Big Data*, 9(1): 109.
- Deng, Y.; Lu, L.; Aponte, L.; Angelidi, A. M.; Novak, V.; Karniadakis, G. E.; and Mantzoros, C. S. 2021. Deep transfer learning and data augmentation improve glucose levels prediction in type 2 diabetes patients. *NPJ Digital Medicine*, 4(1): 109.
- Devlin, J.; Chang, M.-W.; Lee, K.; and Toutanova, K. 2018. Bert: Pre-training of deep bidirectional transformers for language understanding. *arXiv preprint arXiv:1810.04805*.
- Edgar, R. C.; and Flyvbjerg, H. 2015. Error filtering, pair assembly and error correction for next-generation sequencing reads. *Bioinformatics*, 31(21): 3476–3482.
- Faisal, S.; and Tutz, G. 2021. Imputation methods for high-dimensional mixed-type datasets by nearest neighbors. *Computers in Biology and Medicine*, 135: 104577.
- Festag, S.; and Spreckelsen, C. 2023. Medical multivariate time series imputation and forecasting based on a recurrent conditional Wasserstein GAN and attention. *Journal of Biomedical Informatics*, 139: 104320.
- Gelman, A.; Carlin, J. B.; Stern, H. S.; and Rubin, D. B. 2004. *Bayesian Data Analysis*. Chapman and Hall/CRC.
- Goldstein, B. A.; Navar, A. M.; Pencina, M. J.; and Ioannidis, J. P. 2017. Opportunities and challenges in developing risk prediction models with electronic health records data: a systematic review. *Journal of the American Medical Informatics Association: JAMIA*, 24(1): 198.
- Huang, K.; Altosaar, J.; and Ranganath, R. 2019. Clinicalbert: Modeling clinical notes and predicting hospital readmission. *arXiv preprint arXiv:1904.05342*.
- Huang, Y.; Talwar, A.; Chatterjee, S.; and Aparasu, R. R. 2021. Application of machine learning in predicting hospital readmissions: a scoping review of the literature. *BMC medical research methodology*, 21: 1–14.
- Hur, K.; Lee, J.; Oh, J.; Price, W.; Kim, Y.; and Choi, E. 2022. Unifying heterogeneous electronic health records systems via text-based code embedding. In *Conference on Health, Inference, and Learning*, 183–203. PMLR.
- Jarrett, D.; Ceber, B.; Liu, T.; Curth, A.; and van der Schaar, M. 2022. HyperImpute: Generalized Iterative Imputation with Automatic Model Selection.
- Jiang, L. Y.; Liu, X. C.; Nejatian, N. P.; Nasir-Moin, M.; Wang, D.; Abidin, A.; Eaton, K.; Riina, H. A.; Laufer, I.; Punjabi, P.; et al. 2023. Health system-scale language models are all-purpose prediction engines. *Nature*, 1–6.
- Kansagara, D.; Englander, H.; Salanitro, A.; Kagen, D.; Theobald, C.; Freeman, M.; and Kripalani, S. 2011. Risk prediction models for hospital readmission: a systematic review. *Jama*, 306(15): 1688–1698.
- Ke, G.; Meng, Q.; Finley, T.; Wang, T.; Chen, W.; Ma, W.; Ye, Q.; and Liu, T.-Y. 2017. Lightgbm: A highly efficient gradient boosting decision tree. *Advances in neural information processing systems*, 30.
- Lazkecka, M.; Mielniczuk, J.; and Teisseyre, P. 2021. Estimating the class prior for positive and unlabelled data via logistic regression. *Advances in Data Analysis and Classification*, 15(4): 1039–1068.
- Lee, C.; Jo, B.; Woo, H.; Im, Y.; Park, R. W.; and Park, C. 2022. Chronic disease prediction using the common data model: development study. *JMIR AI*, 1(1): e41030.
- Lee, J.; Lee, Y.; Kim, J.; Kosiosek, A.; Choi, S.; and Teh, Y. W. 2019. Set transformer: A framework for attention-based permutation-invariant neural networks. In *International conference on machine learning*, 3744–3753. PMLR.
- Lee, J.; and Park, C. 2022. Restoration of Time-Series Medical Data with Diffusion Model. In *2022 IEEE International Conference on Consumer Electronics-Asia (ICCE-Asia)*, 1–4. IEEE.
- Lewis, S.; Matejovicova, T.; Li, Y.; Lamb, A.; Zaykov, Y.; Allamanis, M.; and Zhang, C. 2021. Accurate imputation and efficient data acquisition with transformer-based vaes. In *NeurIPS 2021 Workshop on Deep Generative Models and Downstream Applications*.
- Li, J.; Yan, X. S.; Chaudhary, D.; Avula, V.; Mudiganti, S.; Husby, H.; Shahjouei, S.; Afshar, A.; Stewart, W. F.; Yeasin, M.; et al. 2021. Imputation of missing values for electronic

- health record laboratory data. *NPJ digital medicine*, 4(1): 147.
- Liberzon, D. 2011. *Calculus of variations and optimal control theory: a concise introduction*. Princeton university press.
- Liu, J.; Allen, P. J.; Benz, L.; Blickstein, D.; Okidi, E.; and Shi, X. 2021. A Machine Learning Approach for Recruitment Prediction in Clinical Trial Design. *arXiv preprint arXiv:2111.07407*.
- Liu, M.; Li, S.; Yuan, H.; Ong, M. E. H.; Ning, Y.; Xie, F.; Saffari, S. E.; Shang, Y.; Volovici, V.; Chakraborty, B.; et al. 2023. Handling missing values in healthcare data: A systematic review of deep learning-based imputation techniques. *Artificial Intelligence in Medicine*, 102587.
- Loshchilov, I.; and Hutter, F. 2017. Decoupled weight decay regularization. *arXiv preprint arXiv:1711.05101*.
- Luo, Y.; Cai, X.; Zhang, Y.; Xu, J.; et al. 2018. Multivariate time series imputation with generative adversarial networks. *Advances in neural information processing systems*, 31.
- Ma, C.; Tschitschek, S.; Palla, K.; Hernández-Lobato, J. M.; Nowozin, S.; and Zhang, C. 2018. Eddi: Efficient dynamic discovery of high-value information with partial vae. *arXiv preprint arXiv:1809.11142*.
- Mahmoudi, E.; Kamdar, N.; Kim, N.; Gonzales, G.; Singh, K.; and Waljee, A. K. 2020. Use of electronic medical records in development and validation of risk prediction models of hospital readmission: systematic review. *bmj*, 369.
- Mazumder, R.; Hastie, T.; and Tibshirani, R. 2010. Spectral regularization algorithms for learning large incomplete matrices. *The Journal of Machine Learning Research*, 11: 2287–2322.
- Padula, W. V.; Kreif, N.; Vanness, D. J.; Adamson, B.; Rueda, J.-D.; Felizzi, F.; Jonsson, P.; IJzerman, M. J.; Butte, A.; and Crown, W. 2022. Machine learning methods in health economics and outcomes research—the PALISADE checklist: a good practices report of an ISPOR task force. *Value in health*, 25(7): 1063–1080.
- Peis, I.; Ma, C.; and Hernández-Lobato, J. M. 2022. Missing data imputation and acquisition with deep hierarchical models and hamiltonian monte carlo. *Advances in Neural Information Processing Systems*, 35: 35839–35851.
- Pierson, E.; Cutler, D. M.; Leskovec, J.; Mullainathan, S.; and Obermeyer, Z. 2021. An algorithmic approach to reducing unexplained pain disparities in underserved populations. *Nature Medicine*, 27(1): 136–140.
- Rao, P. K.; Chatterjee, S.; Nagaraju, K.; Khan, S. B.; Al-musharraf, A.; and Alharbi, A. I. 2023. Fusion of Graph and Tabular Deep Learning Models for Predicting Chronic Kidney Disease. *Diagnostics*, 13(12): 1981.
- Rubin, D. B. 1978. Multiple imputations in sample surveys—a phenomenological Bayesian approach to nonresponse. In *Proceedings of the survey research methods section of the American Statistical Association*, volume 1. American Statistical Association Alexandria, VA, USA.
- Rubinsteyn, A.; and Feldman, S. 2020. fancyimpute: An Imputation Library for Python.
- Sechidis, K.; Sperrin, M.; Petherick, E. S.; Luján, M.; and Brown, G. 2017. Dealing with under-reported variables: An information theoretic solution. *International Journal of Approximate Reasoning*, 85: 159–177.
- Stekhoven, D. J.; and Bühlmann, P. 2012. MissForest—non-parametric missing value imputation for mixed-type data. *Bioinformatics*, 28(1): 112–118.
- Suleiman, M.; Demirhan, H.; Boyd, L.; Giroso, F.; and Ak-sakalli, V. 2020. A clinical coding recommender system. *Knowledge-Based Systems*, 210: 106455.
- Tanner, D.; Morgan-Short, K.; and Luck, S. J. 2015. How inappropriate high-pass filters can produce artifactual effects and incorrect conclusions in ERP studies of language and cognition. *Psychophysiology*, 52.
- Vinas, R.; Zheng, X.; and Hayes, J. 2021. A Graph-based Imputation Method for Sparse Medical Records. *arXiv preprint arXiv:2111.09084*.
- Vivar, G.; Kazi, A.; Burwinkel, H.; Zwergal, A.; Navab, N.; and Ahmadi, S.-A. 2020. Simultaneous imputation and disease classification in incomplete medical datasets using Multigraph Geometric Matrix Completion (MGMC). *arXiv preprint arXiv:2005.06935*.
- Vyas, D. A.; Eisenstein, L. G.; and Jones, D. S. 2020. Hidden in plain sight—reconsidering the use of race correction in clinical algorithms.
- Wang, L.; Qu, L.; Yang, L.; Wang, Y.; and Zhu, H. 2020. NanoReviser: an error-correction tool for nanopore sequencing based on a deep learning algorithm. *Frontiers in Genetics*, 11: 900.
- Wang, Y.; Xu, H.; Xu, Z.; Gao, J.; Wu, Y.; and Zhang, Z. 2022. Multivariate Time Series Imputation Based on Masked Autoencoding with Transformer. In *2022 IEEE 24th International Conference*, 2110–2117. IEEE.
- Wenger, A. M.; Peluso, P.; Rowell, W. J.; Chang, P.-C.; Hall, R. J.; Concepcion, G. T.; Ebler, J.; Fungtammasan, A.; Kolesnikov, A.; Olson, N. D.; et al. 2019. Accurate circular consensus long-read sequencing improves variant detection and assembly of a human genome. *Nature biotechnology*, 37(10): 1155–1162.
- Wu, K.; Dahlem, D.; Hane, C.; Halperin, E.; and Zou, J. 2023. Collecting data when missingness is unknown: a method for improving model performance given under-reporting in patient populations. In *Conference on Health, Inference, and Learning*, 229–242. PMLR.
- Wu, Y.; DuBois, C.; Zheng, A. X.; and Ester, M. 2016. Collaborative denoising auto-encoders for top-n recommender systems. In *Proceedings of the ninth ACM international conference on web search and data mining*, 153–162.
- Yıldız, A. Y.; Koç, E.; and Koç, A. 2022. Multivariate time series imputation with transformers. *IEEE Signal Processing Letters*, 29: 2517–2521.
- Yoon, J.; Jordon, J.; and Schaar, M. 2018. Gain: Missing data imputation using generative adversarial nets. In *International conference on machine learning*, 5689–5698. PMLR.
- You, J.; Ma, X.; Ding, Y.; Kochenderfer, M. J.; and Leskovec, J. 2020. Handling missing data with graph representation

learning. *Advances in Neural Information Processing Systems*, 33: 19075–19087.

Zheng, S.; and Charoenphakdee, N. 2022. Diffusion models for missing value imputation in tabular data. *arXiv preprint arXiv:2210.17128*.

## Proof of Theorem 1

For ease of presentation, we rewrite the theorem below.

**Theorem 2.** Let  $p(\mathbf{x})$ ,  $\mathbf{x} \in \mathcal{X} \subseteq \mathbb{R}^T$ , be the distribution over the data and let  $p(\tilde{\mathbf{x}} | \mathbf{x})$ ,  $\tilde{\mathbf{x}} \in \tilde{\mathcal{X}} \subseteq \mathbb{R}^T$ , be the noise distribution, which we assume is of the following form

$$p(\tilde{\mathbf{x}} | \mathbf{x}) = \beta\delta(\tilde{\mathbf{x}} = \mathbf{x}) + (1 - \beta)q(\tilde{\mathbf{x}} | \mathbf{x}). \quad (7)$$

Moreover, let  $q(\tilde{\mathbf{x}})$  be

$$q(\tilde{\mathbf{x}}) = \int q(\tilde{\mathbf{x}} | \mathbf{x})p(\mathbf{x})d\mathbf{x}, \quad (8)$$

be the marginal distribution of the noisy data. With respect to mean squared error, the optimal denoising function is

$$f_*(\tilde{\mathbf{x}}) = \omega(\tilde{\mathbf{x}})\tilde{\mathbf{x}} + (1 - \omega(\tilde{\mathbf{x}}))g_*(\tilde{\mathbf{x}}) \quad (9)$$

where

$$g_*(\tilde{\mathbf{x}}) \triangleq \mathbb{E}_{q(\mathbf{x}|\tilde{\mathbf{x}})}[\mathbf{x}], \quad (10)$$

$$\omega(\tilde{\mathbf{x}}) \triangleq \frac{p(\tilde{\mathbf{x}})}{p(\tilde{\mathbf{x}}) + \gamma\tilde{q}(\tilde{\mathbf{x}})}, \quad \omega(\tilde{\mathbf{x}}) : \tilde{\mathcal{X}} \rightarrow [0, 1], \quad (11)$$

and  $\gamma \triangleq \frac{1-\beta}{\beta}$ .

*Proof.* To solve for  $f_*$ , we use calculus of variations (Liberzon 2011) but first, we will expand the loss function to make it easier to work with. We start by expanding the MSE and absorbing terms that are not a function of  $f$  into a constant,  $C$ ,

$$\int (f(\tilde{\mathbf{x}}) - \mathbf{x})^\top (f(\tilde{\mathbf{x}}) - \mathbf{x})p(\mathbf{x}, \tilde{\mathbf{x}})d\mathbf{x}d\tilde{\mathbf{x}} \quad (12)$$

$$= \int f(\tilde{\mathbf{x}})^\top f(\tilde{\mathbf{x}})p(\mathbf{x}, \tilde{\mathbf{x}})d\mathbf{x}d\tilde{\mathbf{x}} - 2 \int f(\tilde{\mathbf{x}})^\top \mathbf{x}p(\mathbf{x}, \tilde{\mathbf{x}})d\mathbf{x}d\tilde{\mathbf{x}} + \int \mathbf{x}^\top \mathbf{x}p(\mathbf{x}, \tilde{\mathbf{x}})d\mathbf{x}d\tilde{\mathbf{x}} \quad (13)$$

$$= \int f(\tilde{\mathbf{x}})^\top f(\tilde{\mathbf{x}})p(\mathbf{x}, \tilde{\mathbf{x}})d\mathbf{x}d\tilde{\mathbf{x}} - 2 \int f(\tilde{\mathbf{x}})^\top \mathbf{x}p(\mathbf{x}, \tilde{\mathbf{x}})d\mathbf{x}d\tilde{\mathbf{x}} + C. \quad (14)$$

Dropping the constant,  $C$ , and using the chain rule of probability (Casella and Berger 2021) to rewrite the joint distribution  $p(\tilde{\mathbf{x}}, \mathbf{x})$  as  $p(\tilde{\mathbf{x}}, \mathbf{x}) = p(\mathbf{x})p(\tilde{\mathbf{x}} | \mathbf{x})$ , we have

$$\mathcal{L}(f) \triangleq \int f(\tilde{\mathbf{x}})^\top f(\tilde{\mathbf{x}})p(\mathbf{x})p(\tilde{\mathbf{x}} | \mathbf{x})d\mathbf{x}d\tilde{\mathbf{x}} - 2 \int f(\tilde{\mathbf{x}})^\top \mathbf{x}p(\mathbf{x})p(\tilde{\mathbf{x}} | \mathbf{x})d\mathbf{x}d\tilde{\mathbf{x}}. \quad (15)$$

We will first simplify the **left term** of (15) where we plug in the definition of the noise distribution,  $p(\tilde{\mathbf{x}} | \mathbf{x}) = \beta\delta(\tilde{\mathbf{x}} = \mathbf{x}) + (1 - \beta)q(\tilde{\mathbf{x}} | \mathbf{x})$

$$\int f(\tilde{\mathbf{x}})^\top f(\tilde{\mathbf{x}})p(\mathbf{x})p(\tilde{\mathbf{x}} | \mathbf{x})d\mathbf{x}d\tilde{\mathbf{x}} \quad (16)$$

$$= \int f(\tilde{\mathbf{x}})^\top f(\tilde{\mathbf{x}})p(\mathbf{x})[\beta\delta(\tilde{\mathbf{x}} = \mathbf{x}) + (1 - \beta)q(\tilde{\mathbf{x}} | \mathbf{x})]d\mathbf{x}d\tilde{\mathbf{x}}, \quad (17)$$

$$= \beta \int f(\tilde{\mathbf{x}})^\top f(\tilde{\mathbf{x}})p(\mathbf{x})\delta(\tilde{\mathbf{x}} = \mathbf{x})d\mathbf{x}d\tilde{\mathbf{x}} + (1 - \beta) \int f(\tilde{\mathbf{x}})^\top f(\tilde{\mathbf{x}})p(\mathbf{x})q(\tilde{\mathbf{x}} | \mathbf{x})d\mathbf{x}d\tilde{\mathbf{x}}, \quad (18)$$

$$= \beta \int f(\mathbf{x})^\top f(\mathbf{x})p(\mathbf{x} = \tilde{\mathbf{x}})d\mathbf{x} + (1 - \beta) \int f(\tilde{\mathbf{x}})^\top f(\tilde{\mathbf{x}})q(\tilde{\mathbf{x}})d\tilde{\mathbf{x}}, \quad (19)$$

$$= \beta \int f(\tilde{\mathbf{x}})^\top f(\tilde{\mathbf{x}})p(\tilde{\mathbf{x}})d\tilde{\mathbf{x}} + (1 - \beta) \int f(\tilde{\mathbf{x}})^\top f(\tilde{\mathbf{x}})q(\tilde{\mathbf{x}})d\tilde{\mathbf{x}}. \quad (20)$$

We now move on to the [right term](#) of (15)

$$2 \int f(\tilde{\mathbf{x}})^\top \mathbf{x} p(\mathbf{x}) p(\tilde{\mathbf{x}} | \mathbf{x}) d\mathbf{x} d\tilde{\mathbf{x}} \quad (21)$$

$$= 2 \int f(\tilde{\mathbf{x}})^\top \mathbf{x} p(\mathbf{x}) [\beta \delta(\tilde{\mathbf{x}} = \mathbf{x}) + (1 - \beta) q(\tilde{\mathbf{x}} | \mathbf{x})] d\mathbf{x} d\tilde{\mathbf{x}}, \quad (22)$$

$$= 2\beta \int f(\tilde{\mathbf{x}})^\top \mathbf{x} p(\mathbf{x}) \delta(\tilde{\mathbf{x}} = \mathbf{x}) d\mathbf{x} d\tilde{\mathbf{x}} + 2(1 - \beta) \int f(\tilde{\mathbf{x}})^\top \mathbf{x} p(\mathbf{x}) q(\tilde{\mathbf{x}} | \mathbf{x}) d\mathbf{x} d\tilde{\mathbf{x}}, \quad (23)$$

$$= 2\beta \int f(\mathbf{x})^\top \mathbf{x} p(\mathbf{x} = \tilde{\mathbf{x}}) d\mathbf{x} + 2(1 - \beta) \int f(\tilde{\mathbf{x}})^\top \mathbf{x} q(\tilde{\mathbf{x}}) p(\mathbf{x} | \tilde{\mathbf{x}}) d\mathbf{x} d\tilde{\mathbf{x}}, \quad (24)$$

$$= 2\beta \int f(\tilde{\mathbf{x}})^\top \tilde{\mathbf{x}} p(\tilde{\mathbf{x}}) d\tilde{\mathbf{x}} + 2(1 - \beta) \int f(\tilde{\mathbf{x}})^\top g_*(\tilde{\mathbf{x}}) q(\tilde{\mathbf{x}}) d\tilde{\mathbf{x}}, \quad (25)$$

$$= 2\beta \int f(\tilde{\mathbf{x}})^\top \tilde{\mathbf{x}} p(\tilde{\mathbf{x}}) d\tilde{\mathbf{x}} + 2(1 - \beta) \int f(\tilde{\mathbf{x}})^\top g_*(\tilde{\mathbf{x}}) q(\tilde{\mathbf{x}}) d\tilde{\mathbf{x}}, \quad (26)$$

where  $g_*(\tilde{\mathbf{x}}) \triangleq \mathbb{E}_{q(\mathbf{x}|\tilde{\mathbf{x}})}[\mathbf{x}]$ .

Plugging (20) and (26) into (15), we get

$$\begin{aligned} \mathcal{L}(f) &= \beta \int f(\tilde{\mathbf{x}})^\top f(\tilde{\mathbf{x}}) p(\tilde{\mathbf{x}}) d\tilde{\mathbf{x}} + (1 - \beta) \int f(\tilde{\mathbf{x}})^\top f(\tilde{\mathbf{x}}) q(\tilde{\mathbf{x}}) d\tilde{\mathbf{x}} \\ &\quad - 2\beta \int f(\tilde{\mathbf{x}})^\top \tilde{\mathbf{x}} p(\tilde{\mathbf{x}}) d\tilde{\mathbf{x}} - 2(1 - \beta) \int f(\tilde{\mathbf{x}})^\top g_*(\tilde{\mathbf{x}}) q(\tilde{\mathbf{x}}) d\tilde{\mathbf{x}}. \end{aligned} \quad (27)$$

Using the Euler Lagrange equation (Liberzon 2011), we solve for  $f_*$  by taking a variational gradient of (27) with respect to  $f$  and setting it equal to 0.

$$\frac{\partial \mathcal{L}(f)}{\partial f} = 0 \quad (28)$$

$$2\beta f(\tilde{\mathbf{x}}) p(\tilde{\mathbf{x}}) + 2(1 - \beta) f(\tilde{\mathbf{x}}) q(\tilde{\mathbf{x}}) - 2\beta \tilde{\mathbf{x}} p(\tilde{\mathbf{x}}) - 2(1 - \beta) g_*(\tilde{\mathbf{x}}) q(\tilde{\mathbf{x}}) = 0 \quad (29)$$

$$2\beta f(\tilde{\mathbf{x}}) p(\tilde{\mathbf{x}}) + 2(1 - \beta) f(\tilde{\mathbf{x}}) q(\tilde{\mathbf{x}}) = 2\beta \tilde{\mathbf{x}} p(\tilde{\mathbf{x}}) + 2(1 - \beta) g_*(\tilde{\mathbf{x}}) q(\tilde{\mathbf{x}}) \quad (30)$$

$$\beta f(\tilde{\mathbf{x}}) p(\tilde{\mathbf{x}}) + (1 - \beta) f(\tilde{\mathbf{x}}) q(\tilde{\mathbf{x}}) = \beta \tilde{\mathbf{x}} p(\tilde{\mathbf{x}}) + (1 - \beta) g_*(\tilde{\mathbf{x}}) q(\tilde{\mathbf{x}}) \quad (31)$$

$$f(\tilde{\mathbf{x}}) p(\tilde{\mathbf{x}}) + \frac{1 - \beta}{\beta} f(\tilde{\mathbf{x}}) q(\tilde{\mathbf{x}}) = \tilde{\mathbf{x}} p(\tilde{\mathbf{x}}) + \frac{1 - \beta}{\beta} g_*(\tilde{\mathbf{x}}) q(\tilde{\mathbf{x}}) \quad (32)$$

$$f(\tilde{\mathbf{x}}) \left[ p(\tilde{\mathbf{x}}) + \frac{1 - \beta}{\beta} q(\tilde{\mathbf{x}}) \right] = \tilde{\mathbf{x}} p(\tilde{\mathbf{x}}) + \frac{1 - \beta}{\beta} g_*(\tilde{\mathbf{x}}) q(\tilde{\mathbf{x}}) \quad (33)$$

$$f_*(\tilde{\mathbf{x}}) = \frac{p(\tilde{\mathbf{x}})}{p(\tilde{\mathbf{x}}) + \frac{1 - \beta}{\beta} q(\tilde{\mathbf{x}})} \tilde{\mathbf{x}} + \frac{\frac{1 - \beta}{\beta} q(\tilde{\mathbf{x}})}{p(\tilde{\mathbf{x}}) + \frac{1 - \beta}{\beta} q(\tilde{\mathbf{x}})} g_*(\tilde{\mathbf{x}}) \quad (34)$$

Letting  $\gamma \triangleq \frac{1 - \beta}{\beta}$ ,  $\omega(\tilde{\mathbf{x}}) \triangleq \frac{p(\tilde{\mathbf{x}})}{p(\tilde{\mathbf{x}}) + \gamma q(\tilde{\mathbf{x}})}$  and plugging in the definition of  $g_*(\tilde{\mathbf{x}})$ , we get

$$f_*(\tilde{\mathbf{x}}) = \omega(\tilde{\mathbf{x}}) \tilde{\mathbf{x}} + (1 - \omega(\tilde{\mathbf{x}})) \mathbb{E}_{q(\mathbf{x}|\tilde{\mathbf{x}})}[\mathbf{x}], \quad (35)$$

completing the proof.  $\square$

## Training procedure for Denoise2Impute-T

We train Denoise2Impute-T in a two-stage fashion. First, we train Denoise2Impute,  $g_\theta$ , by minimizing the cross-entropy loss,  $\mathcal{L}$ ,

$$\ell_{CE}(g_\theta(\tilde{\mathbf{x}}), \mathbf{x}) = \sum_{d=1}^T \ell_{ce}(g_\theta(\tilde{\mathbf{x}})_d, x_d), \quad (36)$$

$$\ell_{ce}(g_\theta(\tilde{\mathbf{x}})_d, x_d) = x_d \log g_\theta(\tilde{\mathbf{x}})_d + (1 - x_d) \log(1 - g_\theta(\tilde{\mathbf{x}})_d), \quad (37)$$

where  $x_d$  is the  $d$ -th dimension of  $\mathbf{x}$  and  $g_\theta(\tilde{\mathbf{x}})_d$  is the  $d$ -th dimension of  $g_\theta(\tilde{\mathbf{x}})$ . To place more emphasis on instances where a 0 must be changed to a 1, we modify the cross-entropy loss to be

$$\ell_{CE}(g_\theta(\tilde{\mathbf{x}}), \mathbf{x}) = \sum_{d=1}^T \mathbb{I}[\tilde{x}_d = x_d] \ell_{ce}(g_\theta(\tilde{\mathbf{x}})_d, x_d) + \lambda \mathbb{I}[\tilde{x}_d \neq x_d] \ell_{ce}(g_\theta(\tilde{\mathbf{x}})_d, x_d), \quad (38)$$

where  $\mathbb{I}[\tilde{x}_d \neq x_d]$  corresponds to the case where  $\tilde{x}_d = 0$  and  $x_d = 1$ . In all experiments, we use  $\lambda = 2.0$ . During training, we also randomly mask out dimensions of  $\tilde{\mathbf{x}}$  with probability  $p = 0.3$  as we found it helped with performance.

Fixing  $g_\theta$ , we construct Denoise2Impute-T by introducing a weighting function,  $\omega_\phi$

$$f(\tilde{\mathbf{x}}) = \omega_\phi(\tilde{\mathbf{x}})x + (1 - \omega_\phi(\tilde{\mathbf{x}}))g_\theta(\tilde{\mathbf{x}}) \quad (39)$$

and optimize (38) for  $f$ , i.e.,

$$\ell_{CE}(f_\theta(\tilde{\mathbf{x}}), \mathbf{x}) = \sum_{d=1}^T \mathbb{I}[\tilde{x}_d = x_d] \ell_{ce}(f_\theta(\tilde{\mathbf{x}})_d, x_d) + \lambda \mathbb{I}[\tilde{x}_d \neq x_d] \ell_{ce}(f_\theta(\tilde{\mathbf{x}})_d, x_d), \quad (40)$$

where only  $\phi$  is updated. As  $\omega_\phi$  is not differentiable due to the indicator function, we approximate it during training via the following continuous relaxation

$$\omega_\phi(\tilde{\mathbf{x}}) \approx \sigma(\alpha * (g_\theta(\tilde{\mathbf{x}}) - \phi)), \quad (41)$$

where  $\sigma(\cdot)$  denotes the sigmoid function and  $\alpha$  is a temperature parameter to modulate this approximation. In all experiments, we set  $\alpha = 100$ . Let  $m_j^{00}$  be the average of  $p_{ij}^{00}$  and  $m_j^{01}$  be the average of  $p_{ij}^{01}$  on the training data, for  $j = 1, \dots, T$ . In principle, we want  $m_j^{00}$  to be close to zero and  $m_j^{01}$  to be close to one on the testing data. When optimizing  $\phi$ , we constrain the learned parameters to satisfy  $0 \leq \phi_j \leq m_j^{00}$ .

## Hyperparameters and Architecture Details

### Details of Datasets

For training the denoising model, we begin with two sources of EHR data with overlapping patient populations from a large healthcare institute<sup>1</sup>,  $\mathcal{D}_1 = \{\tilde{\mathbf{x}}_1, \dots, \tilde{\mathbf{x}}_N\}$  and  $\mathcal{D}_2 = \{\tilde{\mathbf{y}}_1, \dots, \tilde{\mathbf{y}}_M\}$ . Each data point is a vector of binary indicators for the presence of ICD-10 diagnosis codes in a patient’s EHR, where we set the number of codes to be 993, i.e.,  $T = 993$ . As  $\mathcal{D}_1$  and  $\mathcal{D}_2$  have overlapping patient populations, we construct the dataset as follows: for patient  $i$  in the common population, we treat the corresponding code vector from  $\mathcal{D}_1$  as the noisy data point,  $\tilde{\mathbf{x}}_i$ . To construct the target code vector,  $\mathbf{x}_i$ , we perform an element-wise OR operation between  $\tilde{\mathbf{x}}_i$  and the same patient’s code vector from  $\mathcal{D}_2$ ,  $\tilde{\mathbf{y}}_i$ ; the OR operation merges any diagnoses that may be unshared between the two data sources. Using the above procedure, a dataset  $\mathcal{D}$  of size 445,345 patients is constructed where 356,276 patients are used for training and 89,069 are used for testing.

### k-NN Details

Let  $\mathcal{B}$  be a subset of patients from the training set of the clean dataset,  $\mathcal{D}$ , that will be used as a buffer. In our implementation, we set  $k = 5$  in all experiments and specify a tolerance  $\tau$ . Given an EHR vector,  $\tilde{\mathbf{x}}$ , we use the Hamming distance to find the closest neighbor in  $\mathcal{B}$ , which we denote by  $\mathbf{x}_n$ . If the Hamming distance between  $\tilde{\mathbf{x}}$  and  $\mathbf{x}_n$  is less than  $\tau$  then all the dimensions in  $\tilde{\mathbf{x}}$  that have a 0 are replaced by the corresponding value in  $\mathbf{x}_n$ . If the Hamming distance between  $\tilde{\mathbf{x}}$  and  $\mathbf{x}_n$  is greater than  $\tau$ , then we keep  $\tilde{\mathbf{x}}$  as is.

### MLP Architecture Details

For the MLP, we used 4 hidden layers, each of width 512, and ReLU activations where a skip connection is added between consecutive layers. The output of the network is then passed through a sigmoid function to ensure they are valid probabilities.

For training, we used the AdamW optimizer (Loshchilov and Hutter 2017) with learning rate  $3.0 \times 10^{-4}$  and a weight decay of  $1.0 \times 10^{-5}$  with a batch size of  $N = 128$ .

### DAE Architecture Details

For the encoder model in denoising auto encoder (DAE), we used 4 fully connected layers, each of width 512, and ReLU activations where a ResNet module is added in the second layer, third layer and fourth layer. The latent dimension of the encoder is 512. For the decoder model of DAE, we used a symmetric architecture as the encoder. The output of the network is then passed through a sigmoid function to ensure they are valid probabilities. We follow the same training method as that for MLP to train the DAE.

### CDAE Architecture Details

We apply the collaborative denoising auto-encoder (CDAE) from Wu et al. (2016) to our noisy data as one baseline. For the encoder model in CDAE, we used 4 fully connected layers, each of width 512, and Tanh activations where an ResNet module is added in the second layer, third layer and fourth layer. The latent dimension of the encoder is 512. The embedding dimension of each patient is 512. For the decoder model of CDAE, we used a symmetric architecture as the encoder. The output of the network is then passed through a sigmoid function to ensure they are valid probabilities. We follow the original implementation of CDAE to set the hyperparameters in our experiment. The corruption ratio is set as 0.5. The learning rate is  $1.0 \times 10^{-3}$ . Adam optimizer is employed to optimize CDAE. The batch size is  $N = 128$ . The number of epochs for training is 50.

<sup>1</sup>To comply with the double-blind submission policy, we withhold the name of the institution providing the datasets; should the paper be accepted, these details will be provided.

## Set Transformer Architecture Details

The shape of input to the Set Transformer is  $(N, T, 1)$ , where  $N$  is the batch size and  $T$  is the number of codes for each patient. We introduce  $T$  learnable embeddings, one for each dimension of  $\bar{\mathbf{x}}$ , where each embedding is of dimension  $D$ . The embeddings are appended with the input leading to a tensor of shape  $(N, T, D + 1)$ .  $L$  layers of the set attention blocks (SABs) are then applied followed by a parallel linear block that maps the output from attention blocks to a tensor of dimension  $(N, T, 1)$ . Finally, a sigmoid function outputs the probability of each code being present. The neural network architecture of  $g_\theta$  is detailed in the Figure 5.

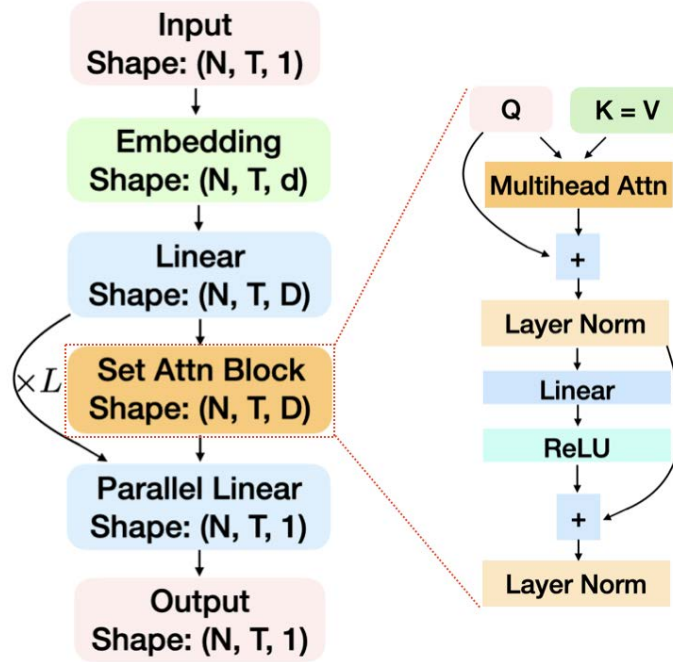


Figure 5: Neural Network Architecture of the denoising model  $g_\theta$ , where one of the key modules is the set attention block (SAB). The tensor shape of outputs in each layer is provided. We apply  $L$  layers of the SAB.

In all our experiments, we set  $D = 200$  and  $L = 4$ , where for each SAB, we set the number of heads to be 10. We use the AdamW optimizer (Loshchilov and Hutter 2017) with learning rate  $3.0 \times 10^{-4}$  and a weight decay of  $1.0 \times 10^{-5}$  with a batch size of  $N = 48$ . All methods in this paper is trained with 50 epochs.

Methods	$\mathcal{D}_1$	Prevalence	MissForest	MLP	CDAE	D2Impute	D2Impute-T
Micro AUPRC	62.67	70.39	64.14	79.10	79.13	81.28	<b>81.64</b>
Macro AUPRC	51.86	52.37	52.23	61.91	62.16	64.89	<b>65.53</b>

Table 2: Micro AUPRC and Macro AUPRC (higher is better) on the test set where noisy vectors were obtained from  $\mathcal{D}_1$ . D2Impute is short for Denoise2Impute.

## Gradient Boosted Tree Details

For the downstream tasks, we used a light gradient boosting decision tree model (LGBM) (Ke et al. 2017) as it had robust downstream prediction performance. In all experiments, we set the hyperparameters of LGBM as follows: `n_estimators = 1000`, `learning_rate = 0.05`, `max_depth = 10`, `reg_alpha = 0.5`, `reg_lambda = 0.5`, `scale_pos_weight = 1`, `min_data_in_bin = 128`.

## Supplementary Experiments

In the following section, we provide additional experimental results where we also investigate how the performance changes when we treat  $\mathcal{D}_2$  as the noisy input instead of  $\mathcal{D}_1$ .

### Details for ICD code prediction task

Given the training set  $\mathcal{D}$ , which consists of 356,276 patients, we used 222,672 patients to train Denoise2Impute and Denoise2Impute-T and the other 133,604 patients are used to train the LGBM model. We selected ICD codes corresponding to seven common chronic conditions: Type-II Diabetes (T2D), Atrial Fibrillation (AFib), Asthma, Chronic Obstructive Pulmonary Disease (COPD), Chronic Kidney Disease (CKD), Hypertensive Heart Disease (HTN-Heart) and Osteoarthritis. We also randomly selected eight additional ICD codes for testing, where we ensured that their prevalence was greater than 6%. The description for the eight randomly selected ICD codes are shown below (Table 3). Here we present detailed results on both, the seven common chronic diseases (Table 4) and the eight randomly chosen codes (Table 5), which correspond to Figure 4A and Figure 4B, respectively.

ICD-10 codes	Description of Diagnosis ICD-10 codes
Z37	Outcome of delivery
Z00	Encounter for general examination without CSRD
Z12	Encounter for screening for malignant neoplasms
M54	Dorsalgia
Z23	Encounter for immunization
Z01	Encounter for other special examination without CSRD
V22	Motorcycle rider injured in collision with two- or three-wheeled motor vehicle
Z34	Encounter for supervision of normal pregnancy

Table 3: Description of additional ICD codes from Fig. 4. CSRD is short for without complaint, suspected or reported diagnosis.

	T2D	AFib	Asthma	COPD	CKD	HTN	Osteoarthritis
Ground Truth	90.77 $\pm 0.14$	58.40 $\pm 0.50$	73.63 $\pm 0.29$	71.59 $\pm 0.46$	80.03 $\pm 0.44$	44.77 $\pm 0.64$	48.76 $\pm 0.32$
$\mathcal{D}_1$	78.47 $\pm 0.14$	40.85 $\pm 0.50$	47.26 $\pm 0.29$	58.08 $\pm 0.46$	61.90 $\pm 0.47$	32.29 $\pm 0.58$	38.13 $\pm 0.31$
softImpute	77.28 $\pm 0.16$	40.06 $\pm 0.48$	46.43 $\pm 0.31$	58.15 $\pm 0.48$	61.78 $\pm 0.51$	32.46 $\pm 0.63$	37.89 $\pm 0.36$
k-NN	78.36 $\pm 0.15$	41.09 $\pm 0.53$	47.42 $\pm 0.17$	58.31 $\pm 0.24$	61.94 $\pm 0.44$	32.23 $\pm 0.64$	38.23 $\pm 0.25$
MLP	78.71 $\pm 0.13$	41.32 $\pm 0.60$	47.69 $\pm 0.22$	58.55 $\pm 0.38$	62.28 $\pm 0.27$	32.02 $\pm 0.54$	38.59 $\pm 0.24$
MLP-T	79.04 $\pm 0.16$	41.59 $\pm 0.57$	47.93 $\pm 0.26$	58.79 $\pm 0.37$	62.75 $\pm 0.32$	32.23 $\pm 0.59$	38.87 $\pm 0.27$
DAE	78.66 $\pm 0.12$	41.38 $\pm 0.55$	47.67 $\pm 0.24$	58.71 $\pm 0.38$	62.41 $\pm 0.33$	32.07 $\pm 0.61$	38.67 $\pm 0.29$
CDAE	78.74 $\pm 0.14$	41.45 $\pm 0.53$	47.64 $\pm 0.27$	58.83 $\pm 0.38$	62.51 $\pm 0.33$	32.11 $\pm 0.42$	38.62 $\pm 0.30$
D2Impute	79.35 $\pm 0.14$	42.11 $\pm 0.52$	47.81 $\pm 0.2$	59.55 $\pm 0.29$	63.05 $\pm 0.42$	32.39 $\pm 0.49$	39.05 $\pm 0.30$
D2Impute-T	<b>79.73</b> $\pm 0.10$	<b>42.74</b> $\pm 0.51$	<b>48.47</b> $\pm 0.29$	<b>60.07</b> $\pm 0.38$	<b>63.85</b> $\pm 0.42$	<b>32.96</b> $\pm 0.52$	<b>39.36</b> $\pm 0.26$

Table 4: Results for 7 ICD codes corresponding to common chronic conditions. Mean AUPRC and 95% confidence interval (CI) are provided. We bootstrap 80% of the test data and repeat 50 times to compute CI. "T2D": type-II diabetes. "AFib": atrial fibrillation. "COPD": chronic obstructive pulmonary disease. "CKD": chronic kidney disease. "HTN": hypertensive heart disease. D2Impute is short for Denoise2Impute.

	Z37	Z00	Z12	M54	Z23	Z01	V22	Z34
Ground Truth	93.86 ± 0.15	90.29 ± 0.07	89.15 ± 0.06	82.5 ± 0.12	78.06 ± 0.09	79.38 ± 0.13	94.81 ± 0.09	93.62 ± 0.16
$\mathcal{D}_1$	80.95 ± 0.31	81.70 ± 0.09	79.81 ± 0.10	82.00 ± 0.09	72.08 ± 0.1	72.28 ± 0.09	75.16 ± 0.31	86.17 ± 0.21
softImpute	80.41 ± 0.33	80.56 ± 0.10	79.32 ± 0.11	81.35 ± 0.10	71.87 ± 0.14	72.41 ± 0.11	75.69 ± 0.32	86.58 ± 0.26
k-NN	80.84 ± 0.32	81.53 ± 0.09	79.95 ± 0.09	82.06 ± 0.10	72.22 ± 0.10	72.43 ± 0.14	75.84 ± 0.29	86.46 ± 0.20
MLP	81.41 ± 0.28	81.71 ± 0.08	80.86 ± 0.07	82.44 ± 0.08	72.86 ± 0.07	72.82 ± 0.14	76.27 ± 0.30	87.0 ± 0.21
MLP-T	81.67 ± 0.31	82.06 ± 0.11	81.02 ± 0.09	82.51 ± 0.07	72.98 ± 0.11	73.05 ± 0.16	76.83 ± 0.35	87.54 ± 0.24
DAE	81.36 ± 0.31	81.83 ± 0.08	80.79 ± 0.09	82.25 ± 0.08	72.79 ± 0.08	72.73 ± 0.14	76.35 ± 0.32	87.12 ± 0.25
CDAE	81.32 ± 0.32	81.89 ± 0.09	80.81 ± 0.10	82.31 ± 0.09	72.75 ± 0.11	72.86 ± 0.12	76.39 ± 0.34	87.08 ± 0.24
D2Impute	81.42 ± 0.30	82.54 ± 0.07	81.27 ± 0.08	82.4 ± 0.09	73.17 ± 0.14	73.37 ± 0.10	77.36 ± 0.28	87.89 ± 0.23
D2Impute-T	<b>82.46</b> ± 0.30	<b>82.75</b> ± 0.07	<b>81.56</b> ± 0.08	<b>82.75</b> ± 0.09	<b>73.54</b> ± 0.07	<b>73.52</b> ± 0.09	<b>78.48</b> ± 0.38	<b>88.47</b> ± 0.18

Table 5: Results for eight randomly chose ICD code predictions, where each ICD code has a prevalence larger than 6%. Mean AUPRC and 95% confidence intervals (CI) are provided. We bootstrap 80% of the test data and repeat 50 times to compute CI. D2Impute is short for Denoise2Impute.

### Benchmarking ICD Code Prediction Tasks using $\mathcal{D}_2$

To investigate how the performance on the ICD code prediction task varies as a function of which noisy dataset we use, we present results for imputation methods where  $\mathcal{D}_2$  is used as the noisy dataset instead of  $\mathcal{D}_1$ . The corresponding AUPRCs are reported in Tables 6 & 7. Compared with Tables 4 & 5, we observe that the absolute value of AUPRC increased across most ICD-10 codes and methods suggesting that  $\mathcal{D}_2$  contains more information that is predictive of  $\mathcal{D}$ , as compared to  $\mathcal{D}_1$ .

	T2D	AFib	Asthma	COPD	CKD	HTN	Osteoarthritis
Ground Truth	90.77 ± 0.14	58.40 ± 0.50	73.63 ± 0.29	71.59 ± 0.46	80.03 ± 0.42	44.77 ± 0.54	48.76 ± 0.32
$D_2$	88.71 ± 0.07	55.38 ± 0.32	71.77 ± 0.18	67.24 ± 0.38	76.02 ± 0.27	41.87 ± 0.68	45.07 ± 0.23
softImpute	86.98 ± 0.14	54.62 ± 0.39	70.06 ± 0.21	66.13 ± 0.41	74.06 ± 0.29	40.14 ± 0.41	43.29 ± 0.24
k-NN	88.16 ± 0.11	54.95 ± 0.38	71.21 ± 0.19	66.88 ± 0.36	75.17 ± 0.33	40.83 ± 0.67	44.26 ± 0.23
MLP	88.82 ± 0.10	55.88 ± 0.39	71.69 ± 0.15	67.82 ± 0.34	76.11 ± 0.28	43.49 ± 0.47	45.78 ± 0.32
MLP-T	89.04 ± 0.15	56.31 ± 0.41	71.95 ± 0.19	68.14 ± 0.37	76.53 ± 0.32	43.72 ± 0.51	46.11 ± 0.34
DAE	88.79 ± 0.12	55.97 ± 0.41	71.76 ± 0.13	68.06 ± 0.36	76.24 ± 0.29	43.38 ± 0.45	45.92 ± 0.35
CDAE	88.87 ± 0.14	56.01 ± 0.45	71.72 ± 0.14	68.24 ± 0.33	76.35 ± 0.31	43.41 ± 0.52	46.03 ± 0.35
D2Impute	<b>89.36</b> ± 0.13	57.32 ± 0.36	72.37 ± 0.15	69.75 ± 0.22	<b>78.11</b> ± 0.25	<b>44.51</b> ± 0.53	<b>47.31</b> ± 0.33
D2Impute-T	89.22 ± 0.12	<b>57.49</b> ± 0.43	<b>72.45</b> ± 0.18	<b>69.99</b> ± 0.35	77.95 ± 0.34	44.50 ± 0.54	47.07 ± 0.36

Table 6: Results for 7 ICD codes corresponding to common chronic conditions. Mean AUPRC and 95% confidence intervals (CI) are provided. We bootstrap 80% of the test data and repeat 50 times to compute CI. "T2D": type-II diabetes. "AFib": atrial fibrillation. "COPD": chronic obstructive pulmonary disease. "CKD": chronic kidney disease. "HTN": hypertensive heart disease. D2Impute is short for Denoise2Impute.

	Z37	Z00	Z12	M54	Z23	Z01	V22	Z34
Ground Truth	93.86 ± 0.15	90.29 ± 0.07	89.15 ± 0.06	82.5 ± 0.12	78.06 ± 0.09	79.38 ± 0.13	94.81 ± 0.09	93.62 ± 0.16
$D_2$	91.98 ± 0.14	89.36 ± 0.06	87.11 ± 0.07	78.28 ± 0.09	75.92 ± 0.10	75.20 ± 0.11	93.95 ± 0.08	90.91 ± 0.15
softImpute	89.74 ± 0.21	87.25 ± 0.09	86.33 ± 0.10	76.44 ± 0.11	73.18 ± 0.14	74.46 ± 0.16	90.16 ± 0.11	88.17 ± 0.18
k-NN	90.22 ± 0.16	88.84 ± 0.07	86.78 ± 0.08	77.83 ± 0.10	76.14 ± 0.13	74.62 ± 0.12	92.75 ± 0.09	90.68 ± 0.16
MLP	92.43 ± 0.17	89.44 ± 0.06	87.44 ± 0.07	78.54 ± 0.13	76.26 ± 0.08	75.47 ± 0.11	93.99 ± 0.12	91.10 ± 0.21
MLP-T	92.78 ± 0.18	89.49 ± 0.08	87.76 ± 0.11	78.95 ± 0.12	76.41 ± 0.10	75.84 ± 0.14	94.11 ± 0.13	91.75 ± 0.19
DAE	92.54 ± 0.19	89.32 ± 0.09	87.49 ± 0.06	78.65 ± 0.18	76.21 ± 0.11	75.56 ± 0.15	93.87 ± 0.14	91.34 ± 0.19
CDAE	92.61 ± 0.16	89.37 ± 0.07	87.56 ± 0.09	78.79 ± 0.16	76.28 ± 0.14	75.74 ± 0.17	93.96 ± 0.13	91.55 ± 0.21
D2Impute	93.41 ± 0.17	89.60 ± 0.05	87.88 ± 0.06	79.79 ± 0.11	76.34 ± 0.10	76.42 ± 0.12	<b>94.48</b> ± 0.13	<b>92.78</b> ± 0.14
D2Impute-T	<b>93.44</b> ± 0.12	<b>89.64</b> ± 0.06	<b>87.93</b> ± 0.08	<b>79.86</b> ± 0.12	<b>76.61</b> ± 0.07	<b>76.50</b> ± 0.14	94.40 ± 0.12	92.77 ± 0.15

Table 7: Results for eight randomly chose ICD code predictions, where each ICD code has a prevalence larger than 6%. Mean AUPRC and 95% confidence intervals (CI) are provided. We bootstrap 80% of the test data and repeat 50 times to compute CI. D2Impute is short for Denoise2Impute.

## Benchmarking Denoising on Hospital Readmission Prediction

We also benchmark the denoising models on a popular healthcare prediction task from the literature, predicting hospital readmission from ICD-10 codes (Kansagara et al. 2011; Huang, Altosaar, and Ranganath 2019; Mahmoudi et al. 2020; Jiang et al. 2023). While ICD-10 codes can be used to predict hospital readmission, the fact that readmission prediction is not an

ICD-10 code itself enhances its credibility as a benchmarking dataset since we no longer need to set a dimension to all 0s before performing denoising. The size of the training dataset is 1,124,550, which is used to train a LGBM model, and the size of the testing dataset is 545,797, which is used to evaluate the performance the LGBM model. We observe that our proposed methods, Denoise2Impute and Denoise2Impute-T, statistically significantly outperform existing imputation methods (Table 8).

Methods	$\mathcal{D}_1$	softImpute	MLP	DAE	CDAE	D2Impute	D2Impute-T
Mean	20.74	18.58	20.81	20.87	20.89	21.47	<b>21.51</b>
CI	$\pm 0.15$	$\pm 0.16$	$\pm 0.13$	$\pm 0.12$	$\pm 0.14$	$\pm 0.10$	$\pm 0.10$

Table 8: Hospital readmission prediction on  $\mathcal{D}_1$  dataset. Mean AUPRC and 95% confidence intervals (CI). We bootstrap 80% of the test data and repeat 50 times to compute CI. D2Impute is short for Denoise2Impute.

### Benchmarking ICD Code Predictions using Synthetic $\mathcal{D}_1$

To investigate how the noise distribution affects the performance of the models, we created an artificial noisy dataset, Noisy  $\mathcal{D}_1$ , from  $\mathcal{D}$ , where the noise was distributed such that the prevalence of Noisy  $\mathcal{D}_1$  matches that of  $\mathcal{D}_1$ . Specifically, a binary mask was randomly sampled per patient and per ICD code and was multiplied with  $\mathcal{D}$ . Results are demonstrated in Figure 6.

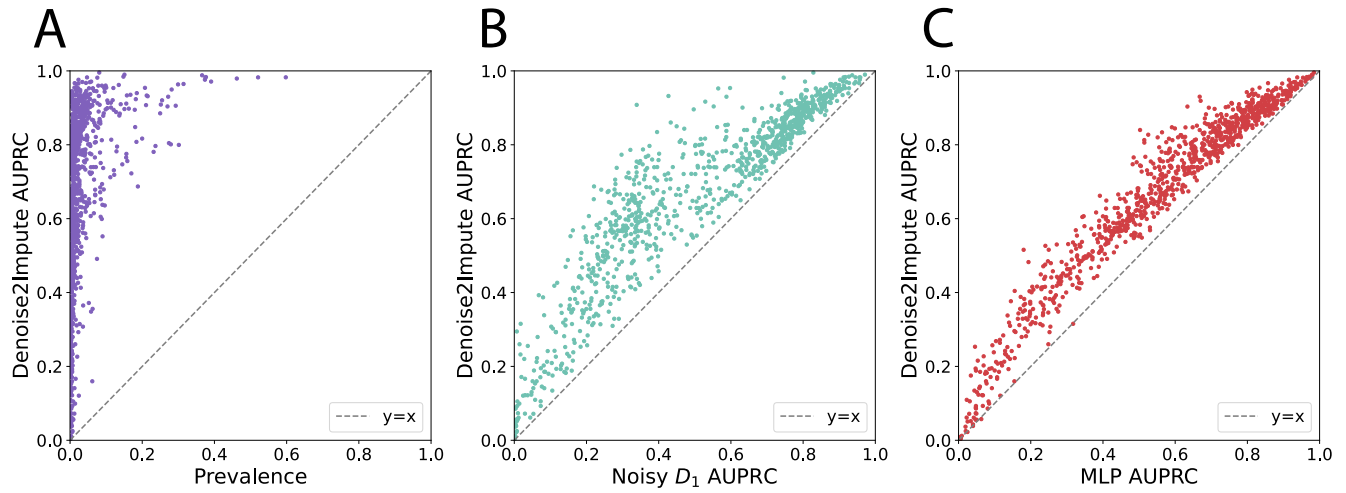


Figure 6: Results on ICD code prediction where the denoising models are trained using Noisy  $\mathcal{D}_1$ . We compare the per ICD code AUPRC of ImputeEHR with those of A) imputing 0's with prevalence B) using Noisy  $\mathcal{D}_1$  and C) denoising using an MLP.